Computational Validation of Thermal Radiation Shielding Effectiveness in Metal Containment Vessels for Small Modular Reactors Using CFD Analysis

Beomjin Jeong [a], Geunyoung Byeon [a], Namgook Kim [a], Sung Joong Kim [a*]
[a]*Department of Nuclear Engineering, Hanyang Univ., 222 Wangsimni-ro, Seongdong-gu, Seoul 04763*
[*]*Corresponding author: sungjkim@hanyang.ac.kr*

***Keywords: SMR, MCV, thermal radiation shielding, emissivity, insulation performance.**

1. Introduction

Small Modular Reactors (SMRs) represent a significant advancement in nuclear technology, offering enhanced safety features, lower capital costs, and modular designs that are well-suited for a range of power generation needs [1]. Among the innovative safety components being explored in advanced SMR designs is the substitution of traditional concrete containment buildings with Metal Containment Vessels (MCVs). The high thermal conductivity of metals, coupled with the absence of insulation, is advantageous for heat removal during accident conditions, but it can lead to significant heat losses during normal reactor operations.

Previous research has highlighted the critical role of thermal radiation in contributing to heat losses under vacuum conditions within the MCV [2]. As part of efforts to reduce heat loss, Thermal Radiation Shielding (TRS) has been proposed as a solution, suggesting that the application of TRS with low emissivity can reduce radiative heat transfer. Figure 1 shows the experimental results from the previous study, illustrating the heat loss ratios for different experimental cases. However, the experimental validation of these findings has been limited.

In this study, we aim to conduct a Computational Fluid Dynamics (CFD) analysis to validate and provide a detailed interpretation of the experimental results previously obtained in evaluating the effectiveness of TRS. This research will not only confirm the experimental results but also offer a deeper understanding of the heat transfer mechanisms involved, contributing to the development of more efficient heat loss reduction strategies for SMRs.

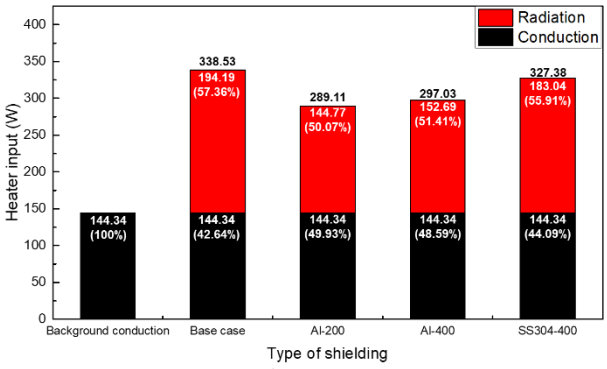

Fig. 1. Conjugate heat transfer in the experimental apparatus according to the experimental case [2].

2. Methodology

2.1. Numerical modeling

In a previous experimental study, the effects of the diameter and emissivity were examined under internal vacuum conditions. In the vacuum, where flow is difficult to develop, it was determined that the heat transfer mechanism of TRS could be accurately analyzed without performing a three-dimensional analysis. Therefore, a two-dimensional axisymmetric method was applied to analyze the performance of TRS. To perform Numerical analysis, a two-dimensional geometry for the computational analysis was created based on the information of the experimental apparatus of the previous study, as shown in Figure 2. Parts of the experimental device that are expected to have a negligible effect on the heat transfer mechanism, such as bolts, nuts, and thin gaskets on the flange, were simplified or merged with similar materials around them.

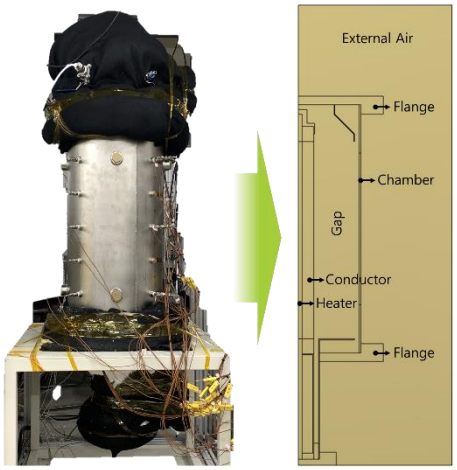

Fig. 2. The geometry for CFD analysis of the experimental apparatus.

The thickness of the TRS used in the experiments are 0.3 mm of the SS304 and 0.2 mm of the Al, and the model includes a TRS geometry with this thickness. The convergence conditions were derived by changing the mesh methodology, and the fabrication methodology for each mesh is summarized in Table 1 below. Since the TRS installation location is different for each case, each mesh was created independently to perform the analysis. Figure 3 shows the mesh for each case.

Table 1: Mesh creation methodology and number of elements

	Background conduction, Base case	Al-200	Al-400	SS304-400
Element Size (m)	0.001			
Defeature Size (m)	5.e-6	5.e-6	5.e-6	5.e-6
Elements number	**767,804**	**767,727**	**768,119**	**768,092**

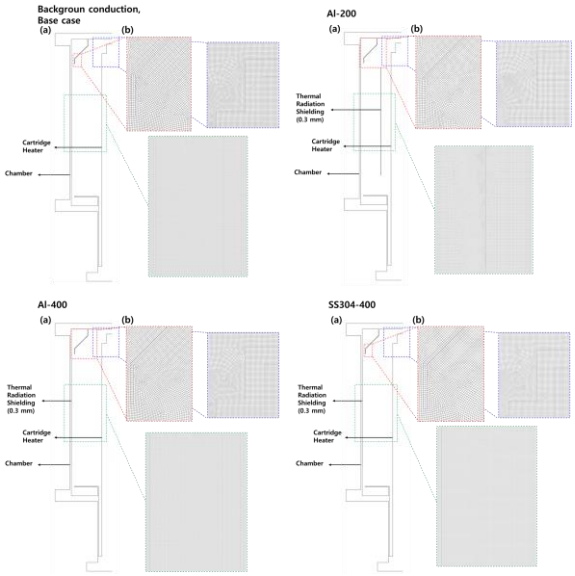

Fig. 3. (a) The two-dimensional axisymmetric geometry of the experimental apparatus and (b) the mesh created from geometry.

The boundary conditions established for this analysis were focused on accurately replicating the experimental conditions. To assist in the interpretation, Figure 4 illustrates the boundary conditions along with each line. First, the temperature of the cartridge heater was set to a constant temperature of 320°C, rather than a constant power input as in the experiment, and the emissivity was set to 0.18 to evaluate the radiative heat transfer from the aluminum heater [3]. Additionally, the emissivity of the inner and outer walls of the chamber, which were made of SS304 and anodized, was set to 0.7. The external air surrounding the chamber was simulated, with the boundary temperature of the external air set to 18°C, consistent with the experimental conditions. The remaining parts were set to adiabatic conditions to simulate the ceramic fiber insulation.

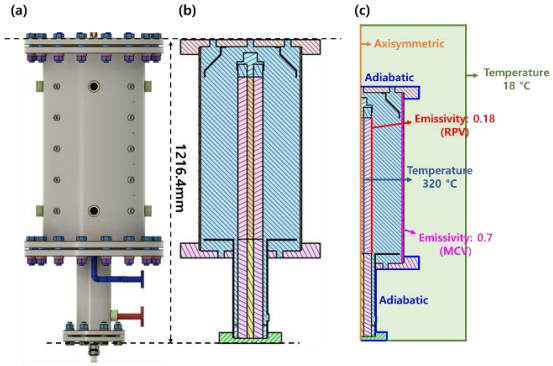

Fig. 4. (a) Experimental apparatus geometry, (b) Geometry cross-section based on the experimental apparatus, and (c) Setting up boundary conditions for a CFD analysis.

To simulate the experimental device in the CFD analysis, the physical properties of the materials used in each area of the device were applied. The cartridge heater and chamber were made of SS304, the conductor wrapped around the cartridge heater was made of aluminum, and the insulation materials located above and below the heater were made of PEEK (Poly Ether Ether Ketone), so their properties were utilized in the simulation. Additionally, background conductive heat loss, which was evaluated by filling the internal gap with ceramic fiber, was simulated in the CFD analysis by applying the properties of ceramic fiber in the gap area. However, ceramic fibers tend to absorb radiation, but to simplify the analysis, the absorption coefficient was not included in this study. Density was expressed as a function of temperature rather than using the Bushnisk approximation to more accurately assess its variation [4]. The materials used in the TRS (Al, SS304) can exhibit differences in emissivity due to surface conditions that vary depending on the processing method. Table 2 summarizes the physical property values of the materials.

Table 2: Materials and physical properties for CFD analysis [5]

Material		ρ [kg/m^3]	μ [kg/m·s]	k [W/m·K]	c_p [J/kg·K]	ε
Vacuum		0.17281 -3.97733x10-4 (T) +2.97726×10-7 (T2)	2.5113e-05	0.03674	1020.5	-
Al	**Conductor**	2719	-	202.4	871	0.18
	TRS					0.04 (Polished)
SS304	**Chamber**	7990		16.3	500	0.7 (Anodizing)
	TRS					0.3 (Lightly oxidized)
Insulator		145		0.1	780	1
PEEK		1183		0.22	0.32	1

2.2. Setting up FLUENT analysis models and solvers

The information about the models and solvers used for analyzing heat transfer mechanisms is summarized in Table 3. The k-omega SST model was employed as the turbulence model. This model is one of the most widely used turbulence models across various engineering fields, known for its reliable performance in diverse flow situations and consistent behavior even in complex geometries and flow phenomena. To simulate radiative heat transfer, we adopted the Discrete Ordinates (DO) model, which is commonly used due to its applicability across all ranges of optical thicknesses and open-top cavities, as well as its reasonable computational cost. Additionally, to further reduce computational costs, gray radiation was assumed, meaning that emissivity does not vary with wavelength, and calculations were performed with a constant emissivity.

Table 3: Comparison of experimental and CFD simulation results: total heat loss for different gap-filling conditions

About FLUENT Analysis Models and Solvers		
Viscous Models		k-omega SST
Radiation Models		Discrete Ordinates (Gray)
Spatial Discretization	**Gradient**	Least Squares Cell Based
	Pressure	Body Force Weighted
	Momentum	2nd Order Upwind
	Energy	2nd Order Upwind
Pressure-based solver		SIMPLE

3. Results and discussions

The convergence criterion for each CFD simulation was evaluated as 10^{-5} or less for the turbulence variables (k and epsilon) and 10^{-6} for the continuity, energy, and DO intensity terms. Based on the results from the simulations that met the convergence criteria, the heat transfer mechanism of the experimental device was analyzed. In the experiment, the total heat loss was evaluated using the input heater power, while in the CFD simulations, it was evaluated based on the heat loss at the boundary of the chamber's external air. To verify the predictive performance, we compared the key result, the final heat loss, as summarized in Figure 5 and Table 4.

Table 4: Comparison of experimental and CFD simulation results: total heat loss for different gap-filling conditions.

	Heater Input (=Total Heat Loss) [W]	
	Experiment [W]	**CFD [W] (Error, %)**
Background conduction	144.34	166.06 (13.1)
Base case	338.53	448.57 (24.5)
Al-200	289.11	333.63 (13.4)
Al-400	297.03	403.37 (26.4)
SS304-400	327.38	434.75 (24.7)

The CFD results show that the total heat loss was predicted to be 13% to 26% higher than in the experiment. This discrepancy was attributed to the boundary condition of the heater, where the entire heater temperature was fixed at 320°C. Despite this, the trend was consistent with the experiment, and the overall error was deemed acceptable, allowing for a detailed analysis based on the defined area of interest. The area of interest was the middle 500 mm of the chamber height in the experimental device, where the TRS is installed. The detailed analysis focused on the total heat transfer from the area of interest to the external air and radiative heat transfer from the gap to the area of interest. Figure 5 provides an illustration to aid in understanding the detailed analysis. Figure 6 shows the temperature and incident radiation distribution of the experimental device for each case.

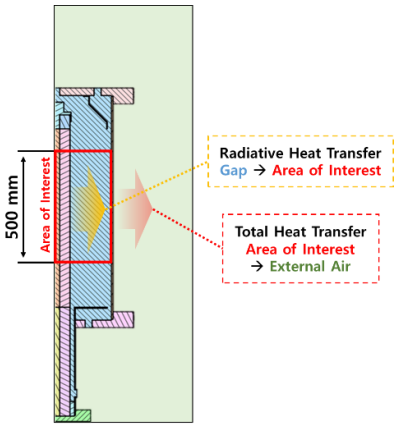

Fig. 5. Illustration for the detailed analysis of heat loss.

3.1. Total heat transfer from Area of interest to external air

Table 5 shows the CFD-calculated total heat loss and the heat loss in the area of interest for each case. Compared to the base case, applying TRS resulted in a reduction of heat loss in the area of interest for all cases. Specifically, with the use of Al-400 TRS, the heat loss in the area of interest was only 40% of the total heat loss. Additionally, the cases with Al-200, Al-400, and SS304-400 TRS showed reductions in heat loss in the area of interest by approximately 34%, 41%, and 15%, respectively, compared to the base case.

Table 5: Comparison of experimental and CFD simulation results: total heat loss for different gap-filling conditions

	Total Heat Loss [W]	**Area of Interest to External Air [W] (portion, %)**
Background conduction	166.06	75.97 (45.7 %)
Base case	448.57	273.45 (61.0 %)
Al-200	333.63	179.87 (53.9 %)
Al-400	403.37	161.46 (40.0 %)
SS304-400	434.75	232.98 (53.6 %)

3.2. Radiative heat transfer from the gap to the area of interest

Table 6 shows the results of CFD calculations for the radiative heat transfer generated in the conductor and the radiative heat transfer that exits through the region of interest. In the base case, a total of 232.99 W of radiative heat is generated from the conductor, with approximately 90% of it escaping to the external air through the region of interest. When TRS of Al-200, Al-400, and SS304-400 were applied, the radiative heat loss through the region of interest was observed to be 58%, 18.5%, and 70.5%, respectively. Comparing the base case with the Al-400 case, there is an approximately 80% reduction in radiative heat loss from the region of interest.

Table 6: Comparison of experimental and CFD simulation results: total heat loss for different gap-filling conditions

	Total Radiative Heat Loss [W]	**Gap to Area of interest [W] (portion, %)**
Background conduction	-	-
Base case	232.99	208.45 (89.5 %)
Al-200	144.13	83.62 (58.0 %)
Al-400	199.33	36.78 (18.5 %)
SS304-400	221.84	156.49 (70.5 %)

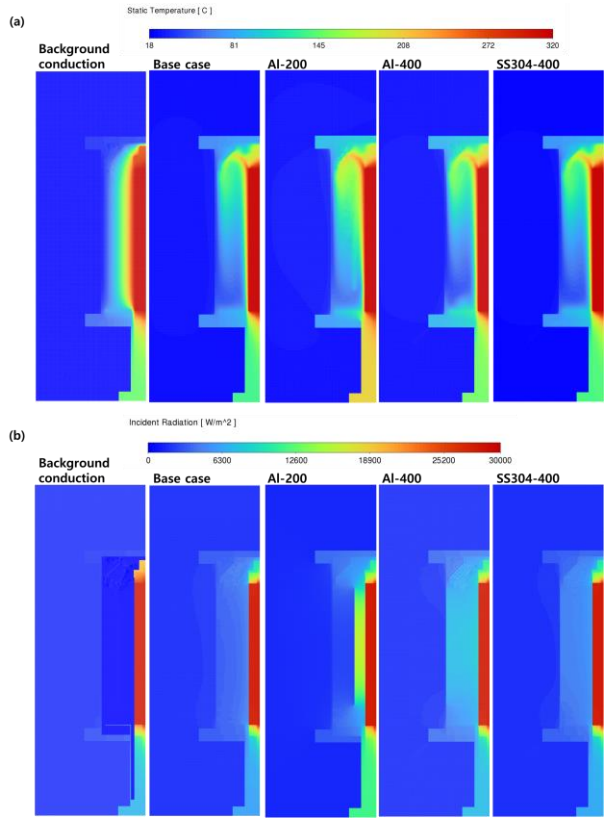

Fig. 6. (a) Temperature and (b) incident radiation contours by TRS type.

4. Conclusion

This study successfully validated the effectiveness of Thermal Radiation Shielding (TRS) in reducing heat loss within Metal Containment Vessels (MCVs) for Small Modular Reactors (SMRs) through Computational Fluid Dynamics (CFD) analysis. The CFD simulations demonstrated that applying TRS significantly reduces both total heat loss and radiative heat transfer from the area of interest to the external air, with the best performance observed in the Al-400 TRS case, which reduced radiative heat loss by approximately 80% compared to the base case. Despite some discrepancies between the experimental and CFD results, particularly due to the fixed heater temperature boundary condition, the overall trends were consistent, indicating that TRS is a viable method for enhancing the thermal efficiency of MCVs in SMRs. This research provides valuable insights into the heat transfer mechanisms involved and contributes to the development of more effective thermal management strategies in nuclear reactor designs.

5. Acknowledgements

This study was sponsored by the Korea Hydro & Nuclear Power Co.'s affiliated Central Research Institute (KHNP-CRI).

This work was supported by the Human Resources Development of the Korea Institute of Energy Technology Evaluation and Planning (KETEP) grant funded by the Korea government Ministry of Knowledge Economy (RS-2024-00439210).

REFERENCES

[1] J. Liou, "What are Small Modular Reactors (SMRs)?", IAEA Office of Public Information and Communication, 2021.
[2] Jeong et al. "An Experimental Study on the Effect of Thermal Radiation Shielding within a Metal Containment Vessel of Small Modular Reactors", Transactions of the Korean Nuclear Society Spring Meeting, Jeju, Korea, May 8–10, 2024.
[3] Ghane, Mohammad and Ghorbani, Ehsan. "Investigation into the UV-Protection of Woven Fabrics Composed of Metallic Weft Yarns" Autex Research Journal, vol. 16, no. 3, 2016, pp. 154-159. https://doi.org/10.1515/aut-2015-0021.
[4] Lee et al., Analysis of heat-loss mechanisms with various gases associated with the surface emissivity of a metal containment vessel in a water-cooled small modular reactor, Nuclear Engineering and Technology, 2024, doi: /10.1016/j.net.2024.03.004.
[5] Y.A. Cengel and A.J. Ghajar, 'Heat and Mass Transfer: Fundamentals and Applications', McGraw Hill, 2015.